Evaluation of Cloud Shading Effects on the Generation and Modification of Mesoscale Circulations

M. SEGAL,* J. F. W. PURDOM,†,# J. L. SONG,* R. A. PIELKE* AND Y. MAHRER†,@

*Department of Atmospheric Science, Colorado State University, Fort Collins, CO 80523,
†Cooperative Institute for Research in the Atmosphere, Colorado State University, Fort Collins, CO 80523 and
#Regional and Mesoscale Meteorology Branch, Development Laboratory, NOAA/NESS, Colorado State University, Fort Collins, CO 80523

(Manuscript received 31 July 1985, in final form 17 October 1985)

ABSTRACT

This study presents scale analysis and numerical model evaluations of the impact of cloud shading on 1) the development of sea breeze and thermally induced upslope flows and 2) the generation of mesoscale circulations between cloudy areas adjacent to clear areas. Based on the assumption of modifications of solar and longwave radiation which are typical for some overcast conditions, it was found that the reduction in the first type of circulation is significant and most noticeable in the vertical velocities. In the second case, thermally induced circulations in favorable conditions appear to approach the typical intensity of the sea breeze.

1. Introduction

In recent years there has been an increasing awareness concerning the potential role that nonclassical thermally induced mesoscale circulations may play in local weather. These types of circulations are related to mesoscale horizontal thermal gradients such as those associated with wet–dry soil contrasts, cloudy areas adjacent to clear areas, snow covered ground next to bare soil, and vegetated soil next to bare soil.

In a previous study, Ookouchi et al. (1984) evaluated the bare soil case, suggesting that for large contrasts of soil wetness along flat terrain, the induced circulations (because of the onset of differential heating) are close in intensity to those of a sea breeze. It is the purpose of the present paper to provide an additional step in the evaluation of the aforementioned circulations by considering the case involved with clouds in which their dynamical interaction with the planetary boundary layer is negligible (i.e., high and medium height clouds as well as elevated stratus or stratocumulus).

Clouds play a major role in determining the amount of both solar radiation and longwave radiation received at the earth's surface. Solar radiation is backscattered and reflected by clouds in addition to some absorption in the cloud layer. This results in a reduction of the direct component and some increase in the fractional contribution of the diffuse component of the solar radiation at the ground surface. The reduction of insolation in overcast areas is well known and may be substantial. On the other hand, clouds often tend to approach longwave blackbody radiators, increasing the net longwave radiation reaching the earth's surface as compared to that received in the clear areas. The loss of solar energy received at the earth's surface because of cloudiness around midday in midlatitudes and the tropics, however, is generally significantly larger than the corresponding increase due to longwave radiation.

The modification of the radiation components in the surface heat balance equation, caused by cloudiness, implies a reduction of the daylight surface temperature in cloudy regions and, therefore, of the magnitude of the surface turbulent heat fluxes. Evaluations of the impact of cloud cover on the surface layer thermal characteristics are summarized, for example, by Oke (1978).

Purdom and Gurka (1974) and Weiss and Purdom (1974) combined daytime satellite observations of cloud cover with surface temperature observations to aid mesoscale surface temperature analyses. In those analyses they found that midday meteorological surface observations of temperature in the cloudy areas were cooler by several degrees Celsius.

The modification of the surface temperature, and correspondingly of the sensible heat fluxes, caused by cloudiness in sea breeze and upslope thermally induced circulations could be expected to cause a significant reduction in the intensity of those circulations. On the other hand, when a daytime cloudiness discontinuity exists (i.e., a cloudy area adjacent to a clear area), a thermally induced mesoscale circulation between the regions should develop. Based on cloud patterns obtained from satellite images and reported observations of surface shelter temperatures, Purdom and Gurka

@ Permanent affiliation: Seagram Centre for Soil and Water Science, Faculty of Agriculture, The Hebrew University of Jerusalem, Rehovot 76100, Israel.

(1974) suggested the existence of such circulations and inferred their possible forcing on subsequent convective cloud development. Purdom (1982) compared the situation to that of the land–sea breeze, i.e., "with the first showers forming in the clear region near the boundary of the early morning cloud cover—a sort of cloud–breeze front." Bailey et al. (1981) applied a three-dimensional numerical model to help explain the occurrence of an intense stationary multicell thunderstorm over London. In that study, shading by an observed layer of medium level clouds was included in the model and found to have an important effect on the resultant weather. The observed severe rainstorm event appeared to be related to a mesoscale circulation that was caused by the thermal contrast that developed between adjacent clear and altostratus cloudy areas. Further discussion of this case is provided in Carpenter (1982). Recently, using a model simulation, McNider et al. (1984) evaluated the initiation of a line of thunderstorms as a result of a mesoscale circulation caused by a horizontal gradient in cloud cover in the morning over Texas. Similar to the earlier studies, he found that early cloud cover played an important role in subsequent thunderstorm development.

The present study is involved with evaluating possible thermally induced mesoscale circulations between cloudy and clear areas, as well as the impact of cloudiness on various other types of thermally induced circulations. It suggests a systematic characterization of these situations; as such it is complementary and a continuation of the earlier studies. A comparative approach is adopted in the presentation and discussion of the results obtained in the present study. Scale analysis is carried out (section 2) to provide insight into the intensity of circulations generated by discontinuities in cloud cover. Additionally, the effect of an overcast on the daytime thermally induced sea breeze circulation and terrain-related upslope flow is evaluated. Numerical model simulations (section 3) were carried out to provide further scaling and to illustrate the aforementioned situations.

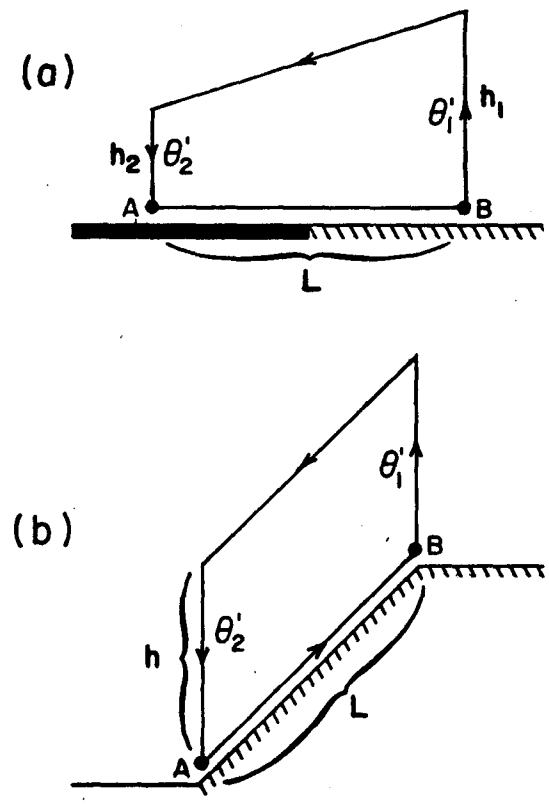

FIG. 1. Schematic illustration of the chosen path of integration for the circulation evaluation: (a) along flat terrain with thermal differentiation; (The dark line indicates a cloudy section.) (b) along a single slope during daytime hours.

2. Scale analysis

In order to provide insight into the expected characteristics of the circulations discussed in section 1, the surface flows were evaluated based on the circulation theorem and following the analysis procedures similar to those in Anthes (1978), Segal et al. (1983) and Ookouchi et al. (1984). Selecting the circulation path illustrated in Fig. 1, we note that the following relations exist:

(i) For the flat terrain case,

$$\frac{\partial C_s}{\partial t} = \frac{\partial}{\partial t}\int_A^B u_s dl \approx \frac{g}{\theta}(h_1\tilde{\theta}_1' - h_2\tilde{\theta}_2') + \int_A^B F(u_s)dl; \quad (1)$$

(ii) For the slope case,

$$\frac{\partial C_s}{\partial t} = \frac{\partial}{\partial t}\int_A^B u_s dl \approx \frac{g}{\theta}\frac{\partial \theta_0}{\partial z}\left(\frac{\partial z_G}{\partial x}\right)Lh - (\tilde{\theta}_2' - \tilde{\theta}_1')\frac{g}{\theta}(h) + \int_A^B F(u_s)dl, \quad (2)$$

where C_s is the line circulation along the surface; u_s is the surface wind component along the circulation path; h is the height of the planetary boundary layer (PBL); L is the horizontal scale of the circulation; θ is potential temperature; g is gravitational acceleration; F is frictional force; $\partial\theta_0/\partial z$ is background potential temperature lapse; $\partial z_G/\partial x$ is slope steepness; ($\tilde{}$) is the vertically averaged value within the PBL depth; and ($'$) is a perturbation from the initial value. It should be noted that in the derivations of (1) and (2) the effect of vertical advection of θ was not considered.

In the derivation of (1) and (2) it was considered that along the upper section of the path (which coincides with the PBL top) the wind speed is zero, while in the lateral sections the vertical wind component

contribution to the circulation is negligible. The horizontal extent of the circulation along a flat terrain is indicated by the section AB, which varies with time along with the PBL height. In the slope case the lateral, vertical segments of the circulation path are fixed at the bottom and at the top of the slope, while the upper segment of the path (along the height of the PBL) varies with time.

Following Tennekes (1973), the height of the PBL, h, at time, t, after sunrise can be approximated by the relation

$$h \approx \left[\frac{2 \int_0^t H_s dt}{\rho_a c_p \frac{\partial \theta_0}{\partial z}} \right]^{1/2}, \quad (3)$$

where H_s is sensible heat flux at the surface, ρ_a air density and c_p specific heat of air at a constant pressure.

It is assumed (as justified in section 3b of this paper) that the sensible heat flux relates linearly through a factor k to the incoming solar radiation at the surface, R_s, less a minimal radiation, r, needed to produce a positive heat flux from the surface to the atmosphere. The value of R_s is the global solar radiation at the surface less the reflected amount of solar radiation. Defining $\bar{R}_s = R_s - r$, then

$$h \approx \left[\frac{2k \int_0^t \bar{R}_s dt}{\rho_a c_p \frac{\partial \theta_0}{\partial z}} \right]^{1/2}. \quad (4)$$

The PBL averaged perturbation of the potential temperature from that of the initial potential temperature within the PBL depth is given by the following approximation:

$$\tilde{\theta}'(t) \approx \frac{1}{2} h \left(\frac{\partial \theta_0}{\partial z} \right). \quad (5)$$

The friction term is presented for the scaling purposes of this study in its Rayleigh form as

$$F(u_s) = -\alpha u_s. \quad (6)$$

Assuming that $\int_A^B u_s dl$ (and also u_s) change linearly with time, then Eq. (1) and the relations (4)–(6), provide an estimation of its magnitude after time t from the initiation of the circulation:

$$\int_A^B u_s dl \approx \frac{kt}{\left(1 + \frac{1}{2}\alpha t\right)} \frac{g}{\theta} (\rho_a c_p)^{-1} \int_0^t (\bar{R}_{s_1} - \bar{R}_{s_2}) d\tau. \quad (7)$$

Similarly, in the slope case, Eq. (2) can be approximated as

$$\int_A^B u_s dl \approx \left[\frac{kt}{\left(1 + \frac{1}{2}\alpha t\right)} \left(\frac{g}{\theta} \frac{\partial z_G}{\partial x} \right) \right] \times \left[k \frac{\partial \theta_0}{\partial z} (\rho_a c_p)^{-1} \int_0^t \bar{R}_s d\tau \right]^{1/2} L. \quad (8)$$

In the derivation of (8) the second term in (2) was not considered because of its negligible magnitude, as compared to the first one. From scaling consideration the ratio of these two terms is

$$(\tilde{\theta}'_2 - \tilde{\theta}'_1)/(\theta_{0_2} - \theta_{0_1}) \approx O(10^{-1}).$$

The analysis presented heretofore is conceptually appropriate for clear sky situations or in situations where clouds exist above the PBL top (e.g., medium and high level clouds). When the PBL is capped by a cloud deck (e.g., stratus), the result is net longwave radiative cooling of the cloud layer. The longwave radiative cooling may reach values of 50 W m^{-2} as observed, for example, by Nicholls (1984). Comparing it with surface sensible heat fluxes computed in section 3c for cloudy cases suggests that the longwave radiative cooling may become an additional important factor to be considered in the bulk evaluation of the PBL. Overall in such cases, a shallower and cooler PBL would result as compared to the case with an equivalent cloud which exists above the PBL top.

As related to the present study, it is suggested that when a relatively thin cloud layer exists atop the PBL, the circulation generation/modification evaluated by the analysis and the simulations presented in section 3 are not altered significantly. On the other hand, in cases of thick cloud layer capping the PBL, it is suggested the above circulation characteristics are somewhat enhanced as compared to those evaluated in the present study.

3. Simulations

a. Model aspects

The formulation of the numerical mesoscale model utilized in the current study is given in detail in Pielke (1974), Mahrer and Pielke (1977), and McNider and Pielke (1981) and therefore will not be repeated here. The model used in this study (2-D version) consists of 14 levels from the near-surface to 7000 m. (Model levels for potential temperature and specific humidity computations are given in Table 1; the computation levels for the wind velocity are staggered with respect to the θ levels.) The model input parameters are the same as those tabulated in Mahrer and Pielke (1977). The numerical time step for the simulations in this study is 50 s. The initial conditions for temperature and specific humidity used in the various simulations are given in Table 1. These conditions consist of a relatively moist planetary boundary layer (PBL) capped with a slight

TABLE 1. The initial vertical profiles of the potential temperature (θ) and the specific humidity (q) at the beginning of the various model simulations.

	Level (m)													
Parameter	10	32.5	75	200	400	600	800	1050	1350	1750	2500	4000	6000	7000
θ (°K)	298.8	299.4	299.8	299.8	300.0	300.2	300.4	304.2	306.2	308.3	314.7	322.1	329.9	333.8
q (gr/kg)	17.2	16.9	16.9	15.0	14.0	13.0	8.5	8.0	5.5	4.2	1.2	1.2	1.2	1.2

upper layer inversion and represent typical August conditions in the subtropical latitudes.

It is worth noting that validation studies of the current model (e.g., Pielke and Mahrer, 1978; Segal and Pielke, 1981; Segal et al., 1982; Abbs, 1984) indicated skill in the capability of the model to resolve mesoscale amospheric features. Those studies should provide some confidence as to the accuracy of the current simulations.

b. *Radiation aspects*

Numerous theoretical and observational studies have evaluated the impact of a cloudy atmosphere on short and longwave radiation. The parameterization of radiation for atmospheric numerical models was reviewed most recently by Stephens (1984). The current study, however, is oriented toward a general evaluation and scaling of the circulation features as outlined in section 2. The net radiation at the surface, which can be approximated adequately by simplified relations, is the main forcing of relevance to these circulation features. Therefore, it is justified to adopt in the context of the present study a simplified approach in the representation of the modifications of the surface radiation in a cloudy atmosphere.

The modified longwave radiation at the surface due to clouds, L_m, was approximated according to a general relationship (e.g., Oke, 1978):

$$L_m = L_c(1 + ac^2), \tag{9}$$

where L_c is the incoming longwave radiation at the surface on a clear day; c is the fraction of sky covered by clouds (which in the present study was assumed to be related to the amount of reduction in the incoming solar radiation at the surface) and a is a constant relating to the cloud type. In our simulations $a = 0.22$, which is a typical value given in Oke (1978) for stratiform cloud cases. The solar radiation at the surface was prescribed as outlined in the description of the simulations presented in subsections 3c, d.

c. *One-dimensional sensitivity simulations*

In order to provide insight into the impact of cloudiness on mesoscale circulations, a series of one-dimensional model simulations were carried out for various reductions of solar radiation reaching the surface (ranging from clear sky to a solar radiation reduced to 20% of the clear sky radiation). A geostrophic flow of 4 m s^{-1} was assumed for these integrations. (This speed is on the order of the mesoscale-induced circulations presented later.) The pattern of the sensible heat fluxes at the surface and the air temperature at 2 m during the daytime are shown in Fig. 2. (The temperatures at this height were interpolated using the surface-layer similarity temperature profile function along with the surface temperature and the first level of the model's predicted temperature.) Two soil wetness situations were assumed: 1) relatively dry soil with a soil moisture availability of 0.05; (This case was also adopted for the two-dimensional simulations reported in the subsection d.) and 2) relatively wet soil with a soil moisture availability of 0.5. The soil moisture availability is defined as the ratio of the surface evaporation rate to the potential evaporation rate at the surface. As such it provides an indication of the relative wetness of the soil.

Figure 2a shows that for a relatively dry soil in the simulated case, when cloudiness diminishes the incoming solar radiation at the surface to 20% of the clear sky radiation, the sensible heat flux is reduced by one order of magnitude. The relative change in heat flux associated with the wet soil is even larger. The increased surface latent heat fluxes in the wet soil cases, in general, substantially reduce the sensible heat fluxes as compared to the corresponding cases involving the dry soil.

Figure 2b shows the resulting patterns of the air temperature at 2 m. The daytime peak temperatures in the dry soil case are larger in the clear sky case by about 7°C as compared to the case in which the solar radiation at the surface is reduced to 20%. This difference becomes less for the wet soil case. The decrease of the sensible heat fluxes in the wet soil cases leads to a reduction in the air temperature as compared to the dry soil cases. This reduction in air temperature is smaller with the cloudy cases (e.g., only 1°C less over the wet soils for the 20% solar insolation cases) as compared with the less cloudy cases (e.g., about 4.5°C less in the clear sky cases).

Based on the one-dimensional simulations (outlined above), the functional relationship between incoming solar radiation at the surface, R_s, and the sensible heat flux, was evaluated for relatively dry and wet soils. Figure 3 shows that a linear relation exists between both parameters, as adopted in the derivation of Eq. (4).

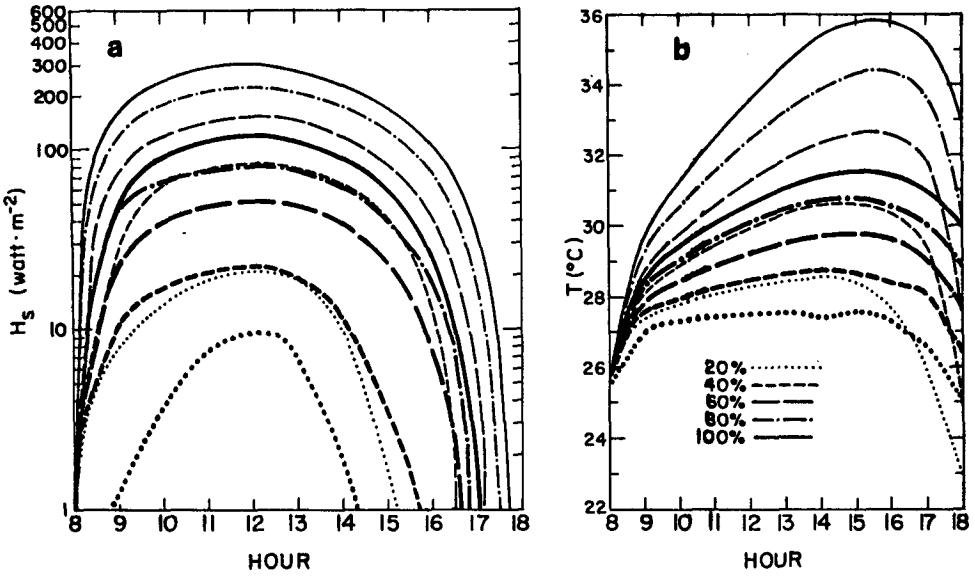

FIG. 2. Temporal variation of the (a) sensible heat fluxes (H_s) and (b) the air temperature at 2 m, for various fractions (as indicated in percent) of a clear sky solar radiation incoming to the surface, as obtained by one-dimensional model simulations. Thin curves indicate dry soil simulations (soil moisture availability = 0.05); thick curves indicate wet soil simulations (soil moisture availability = 0.5).

This type of linear relation was also found to exist when the wind speed was changed from that stated earlier. For the dry soil cases the minimal solar radiation needed to produce a sensible heat flux from the surface to the atmosphere, r, is about 100 W m^{-2}, while for the wet soil cases $r \approx 200$ W m^{-2}. The range of R_s which is typical for the simulations described in subsection 3d is 550–800 W m^{-2} for the clear-sky areas. For the dry soil case $H_s \approx 0.5\bar{R}_s$, while for the wet soil $H_s \approx 0.16\bar{R}_s$. Thus, for the circulations evaluated in Eqs. (7) and (8) $k \approx 0.5$ for the dry soil case and 0.16 for the wet soil case. This implies a substantially stronger corresponding circulation with dry soil cases as compared to those involved with wet soil cases.

d. Two-dimensional simulations

The two-dimensional simulations, using the initial profile of potential temperature and specific humidity in Table 1, were carried out using a horizontal grid interval of 3 km. They consisted of a set of experiments designed to evaluate the impact of cloudiness on the development of sea breeze and daytime thermally induced upslope flows. Another set of experiments was designed to examine the development of circulations involved with cloudiness contrasts for several hypothetical situations. A description of the 2-D simulated cases is given in Table 2.

In these simulations it was assumed that the incoming solar radiation at the surface in the cloudy areas was reduced to 40% of its value under clear sky con-

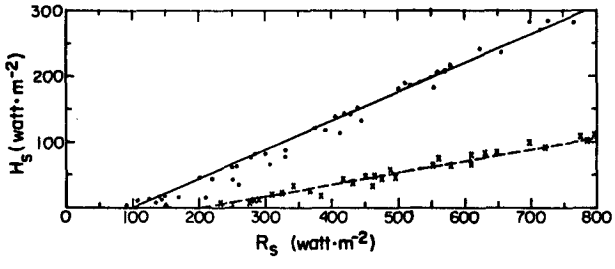

FIG. 3. The relation between the sensible heat flux (H_s) and the solar radiation incoming to the surface (R_s) based on the various simulations used in Fig. 2. Solid line indicates a dry soil case (soil moisture availability = 0.05); dashed line indicates a wet soil (soil moisture availability = 0.5).

TABLE 2. Description of the two-dimensional simulated cases. In cloudy domain section the incoming solar radiation at the surface is 40% of its amount in the clear area.

Simulated case	Description
SBN	Sea breeze without clouds
SBC	Sea breeze with clouds
SN	Upslope flow without clouds
SC	Upslope flow with clouds
CCC	Cloudy area contrasted by clear area
CCD	Cloudy area contrasted with clear area; cloud dissipation (or advection of clouds away from the clear area)
CCA	Cloudy area contrasted with clear area; cloud advection to the clear area
C10	Cloudy area contrasted with clear area beginning at 1000 LST
C12	Cloudy area contrasted with clear area beginning at 1200 LST
C14	Cloudy area contrasted with clear area beginning at 1400 LST

ditions. Under overcast sky conditions this amount of reduction in solar radiation can be representative for several types of clouds mentioned in section 1 (e.g., see Liou, 1976). A weak synoptic flow (0.5 m s^{-1}) and dry soil conditions (0.05 soil moisture availability) were assumed in these experiments. A summary of selective typical features obtained in the two-dimensional simulations are given in Table 3.

1) SEA BREEZE CASE

Sea breeze circulations in subtropical and midlatitudes are known to be one of the major factors in determining local coastal weather during the warm season. In many locations it may be readily recognized by the development of cumulus clouds involved with the sea breeze front, as, for example, over Florida. In some cases the sea breeze development may become modified by preexisting clouds, such as multilayered cloudiness accompanying the passage of a synoptic system, a band of cirrus associated with the subtropical jet stream, or cirrus debris from nocturnal thunderstorm activity.

In an observational study, Gannon (1978) found that the sea breeze was essentially eliminated when thunderstorm-generated anvils shaded the south Florida Peninsula. Such situations are examined through the results of the two-dimensional simulations as described in the following paragraphs.

By 1400 LST, a time at which the sea breeze (SB) approaches its peak flow intensity, the SB in the clear case (SBN) penetrated about 40 km inland as compared with only 27 km in the corresponding cloudy case (SBC) (Fig. 4a, b). Highest values of the u component (in the cross-shore direction) at the time are above 6 m s^{-1} in the clear situation versus about 4 m s^{-1} in the cloudy case.

The reduction in the vertical velocity along the sea breeze front in the cloudy case (Fig. 4c, d) is remarkably large. The sea breeze low-level convergence is substantially reduced as compared to equivalent situations on a clear day.

The decrease of the onshore potential temperature for the cloudy case is about 4°C in the suface layer and about 1°C at 1000 m as compared to the clear case (Fig. 4e, f). This implies a substantial reduction in the horizontal pressure gradient involved with the circulation. It is worth noting the decrease of the onshore PBL depth from a typical value of about 1500 m in SBN to 1000 m in SBC (as evident from the vertical structure of θ in Fig. 4e, f). This reduction suggests, for example, a significant decrease in the PBL depth as well as in the ventilation volume for pollutants on cloudy days along coastal areas where the SBN flow dominates the synoptic flow. In case SBN the perturbation of the isentropes in the location of the cold front (Fig. 4e) is very noticeable.

2) SLOPED TERRAIN CASE

Similar simulations to those described in the sea breeze case were carried out for a sloped terrain case. The simulated terrain has a west facing slope of 1/30, with an elevated plateau to the east.

In many mountainous regions afternoon and evening convective activity is supported by a daytime circulation (e.g., studies for the United States by Dirks, 1969; Wallace, 1975; Klitch et al., 1985, among others). Hence, the existence of cloud shading during the first half of the day should contribute to a reduction in the intensity of upslope flow circulations, and possibly a reduction in thunderstorm activity.

Figures 5a, b illustrates the effect of shading on the u component of the upslope flow at 1400 LST. In both cases the circulation penetrates to the plateau. The typical surface level flow at the middle of the slope is 5–6 m s^{-1} in the clear case (SN), as compared to 3 m s^{-1} in the cloud case (SC). The stronger upslope flows simulated in the case SN imply that in the existence of an opposing synoptic flow, the generated local convergence zone in a clear sky condition should be more pronounced than in cloudy cases. Banta (1984) studied such convergence zones in the Rocky Mountains. He suggested that such convergence zones in that area provide an important mechanism for the initiation of mountain-generated cumuli and their continued growth into cumulus congestus and cumulonimbus clouds.

The vertical velocities reach their peak values along the top of the slope and at the edge of the circulation over the plateau. The latter peak values are substantially lower in the cloudy case (Fig. 5c, d). The decrease in depth of the PBL along the slope in the cloudy case as indicated by the potential temperature patterns (Fig. 5e, f) is about 60% of that of the clear case. This reduction is in good agreement with the value estimated using Eq. (4) based on radiation considerations. [At

TABLE 3. Several typical features obtained in the two-dimensional simulations following t (seconds) from their commencement. w_{max} indicates the maximum vertical velocity at the simulated cross section; $u_{s\,max}$ indicates the maximum u component at 5-m height at the simulated cross sections; C_m and C_a are the simulated and analyzed surface line circulations, respectively. (Computation of C_a values in cases CCD and CCA requires further refinements in the formulation given in section 2.)

Case	w_{max} (cm s^{-1})	$u_{s\,max}$ (m s^{-1})	t (s)	C_m (m^2 s^{-1})	C_a (m^2 s^{-1})
SBN	35	5.8	21600	$2.42 \cdot 10^5$	$2.44 \cdot 10^5$
SBC	10	3.6	21600	$1.11 \cdot 10^5$	$0.76 \cdot 10^5$
SN	22	5.8	21600	$1.47 \cdot 10^5$	$1.41 \cdot 10^5$
SC	14	3.8	21600	$1.06 \cdot 10^5$	$0.80 \cdot 10^5$
CCC	28	4.5	21600	$1.27 \cdot 10^5$	$1.08 \cdot 10^5$
CCD	17	3.1	21600	$1.15 \cdot 10^5$	—
CCA	27	4.2	21600	$1.16 \cdot 10^5$	—
C10	14	3.2	7200	$0.32 \cdot 10^5$	$0.37 \cdot 10^5$
C12	22	3.1	7200	$0.33 \cdot 10^5$	$0.39 \cdot 10^5$
C14	20	2.7	7200	$0.30 \cdot 10^5$	$0.27 \cdot 10^5$

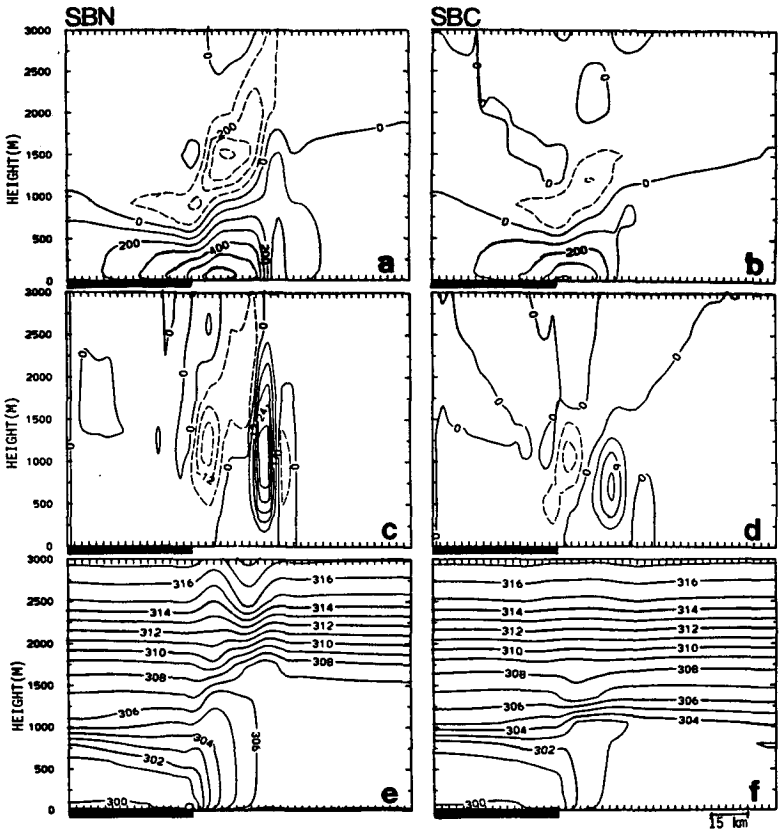

FIG. 4. Vertical cross section of the simulated domain for the cases SBN and SBC at 1400 LST for (a) and (b) u (west–east) component of the wind in cm s^{-1}; (Dashed contours indicate negative component-easterly.) (c) and (d) the vertical wind component in cm s^{-1}; (Dashed contours indicate negative component-downward vertical velocity.) (e) and (f) the potential temperature in °K. The dark segment indicates the sea section of the domain.

the given hour $(R_s)_N$ over the clear-sky slope is about 700 W m^{-2}, yielding $(\bar{R}_s)_N \approx 700-100 = 600$ W m^{-2}; for the cloudy slope $(R_s)_C \approx 280$ W m^{-2}, resulting in $(\bar{R}_s)_C \approx 280-100 = 180$ W m^{-2}. The ratio between the cloudy and clear-sky slope PBL depth is given using (4) as $\{(\bar{R}_s)_C/(\bar{R}_s)_N\}^{1/2} = 0.55$).] It is worth noting that the approximate coincidence of the $u = 0$ contour in Fig. 5a, b with the height of the PBL as implied by the simulation results in Fig. 5e, f, was assumed in the analysis of section 2. The reduction to zero of the u component at some level above the surface is often anticipated when a background flow prevails, since it either opposes the lower-layer thermally induced flow or the return flow aloft.

3) CLOUDY AREA–CLEAR AREA CONTRASTS

In order to provide a qualitative evaluation of the circulation involved with clear ground adjacent to a cloud area, three simulations were performed. In the first simulation (case CCC) it was assumed that the cloud cover persists during the whole simulation and its location is fixed. This is similar to the case shown by Purdom (1982) using GOES imagery, although in that case the early cloud cover was observed to dissipate during the day. The results for the u component in the vertical cross section indicate only slightly lower peak values in this case (Fig. 6a) as compared to that obtained in the clear sky sea-breeze simulation (case SBN) (Fig. 4a). The horizontal extent of the circulation in the SBN case, therefore, is noticeably larger than that in the current case, as implied from Eq. (7) and the larger horizontal radiation difference involved with the SBN case (see Table 3). As indicated by the potential temperature field (Fig. 6c), the atmosphere over the cloudy section has gained sensible heat. This causes the PBL layer to be warmer and deeper than that simulated in the SBN case over the sea section. The vertical velocities (Fig. 6b) in the front location (which differ by 10 km between the two cases) are somewhat smaller than those simulated in the SBN case.

Generally, contrast lines separating cloudy and clear areas change their locations because of advection, dissipation, or formation of clouds. Hence, case CCC reflects an ideal situation, intended mostly to provide comparison with the sea breeze simulations. The next

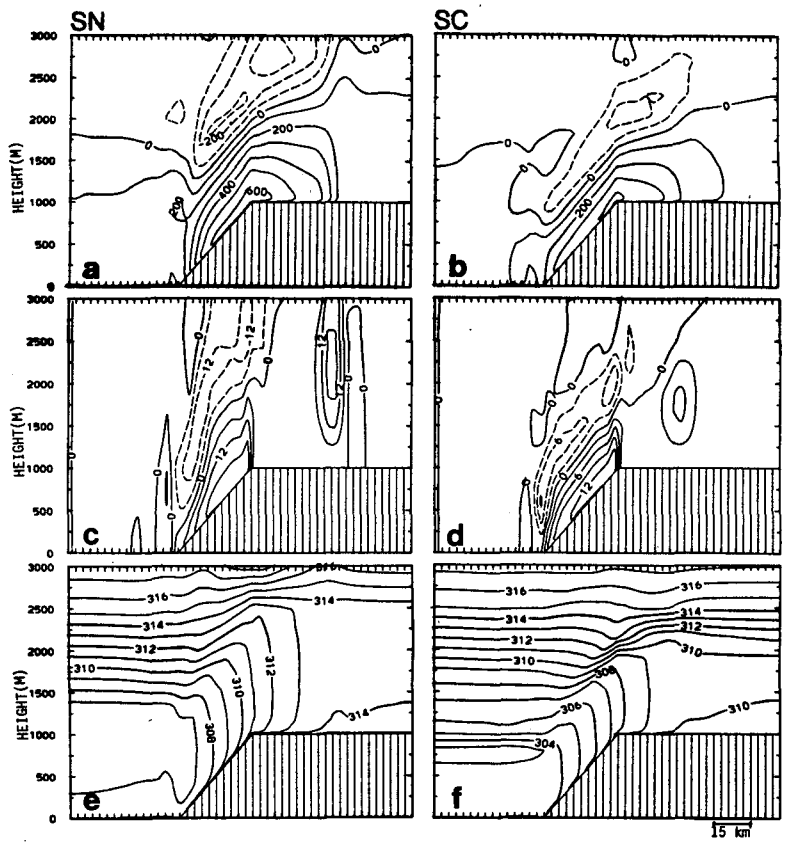

FIG. 5. Vertical cross section of the simulated domain for the cases SN and SC at 1400 LST for (a) and (b) u (west–east component of the wind in cm s^{-1}; (Dashed contours indicate negative component-easterly.) (c) and (d) the vertical wind component in cm s^{-1}; (Dashed contours indicate negative component-downward.) (e) and (f) the potential temperature in degrees Kelvin.

two cases (CCD and CCA) are involved with movable contrast lines.

Dissipation of stratus clouds covering large areas following sunrise has been observed to progress from the edge of an overcast area inward (e.g., Gurka, 1978). The subsidence involved with the circulation generated by the clear–cloud contrast itself could be the cause for this observation. A simulation result reflecting an analogous situation is given in Fig. 7 (CCD). The simulation is similar to the previous case except for the change in the location of the cloud cover. The cloudiness was removed on the left at a speed of 6 km h^{-1}, providing a representation of a progressive dissipation of the cloudiness as described above or, alternatively, its advection. The shaded sections in Fig. 7 indicate the expansion of the clear area from the beginning of the simulation to the presented hour. Erosion of the cloud lateral boundary in the opposite direction to that of the circulation zone should reduce the circulation intensity as compared to the case CCC. The results in Fig. 7a, c do indeed indicate a reduction of the u and w components as compared to the stationary cloud cover case. The vertical velocity cells (particularly that of the downward velocities) are wider than those involved with the previous case. The horizontal thermal gradients (Fig. 7e) along the contrast line are, as expected, slightly weaker as compared with case CCC. Increasing the speed of the contrast line movement contributed to an additional reduction in the horizontal thermal gradient and further reduction in the peak velocities generated by the circulation (not shown).

The advection of clouds toward a clear area is considered in the third simulation (CCA) where the cloudy area was steadily shifted toward the clear area. The simulation provides an analogy, for example, to the advection of middle and high level clouds in that direction, while the lower atmosphere is relatively calm. Results, which are obtained using a simulated cloud movement speed of 6 km h^{-1}, are shown in Fig. 7 (CCA). Progression of the cloud cover in the same direction as that of the circulation front helps increase the distance the front of the cold air mass moves as compared to that involved with a stationary cloudy area. The horizontal and vertical velocities obtained

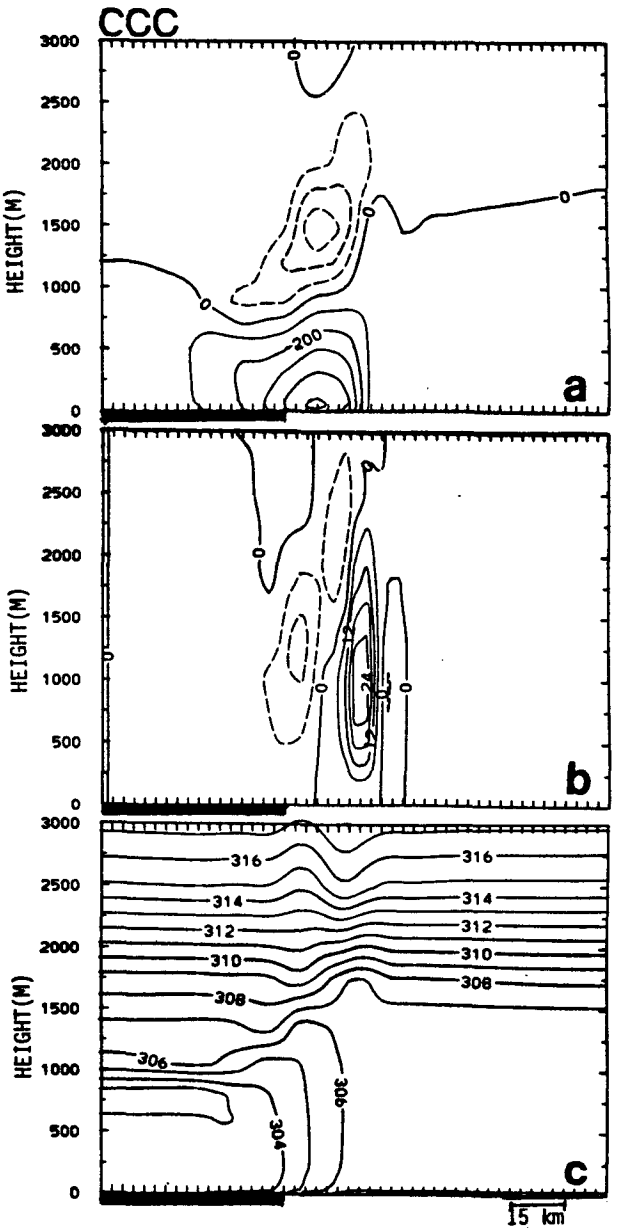

FIG. 6. As in Fig. 4 except for case CCC. The cloudy section is indicated by a heavy, dark line.

are similar to those obtained in the case CCC. The horizontal thermal gradient (Fig. 7f) shows some intensification in the location adjacent to the edge of the cooler air mass.

With a sea breeze, in the absence of synoptic flow, the rate of inland progress of the sea breeze front is in the range of 5–10 km h^{-1} (e.g., Neumann and Mahrer, 1974; Simpson et al., 1977). However, it may be lower around noon as reflected by the results of the current simulations. Increasing the speed of the contrast line in this case beyond 6 km h^{-1} is expected to cause a decay in the development of the circulation flows, since cloud shadowing overruns the zone of maximum thermal gradient.

4) SHORT PERIOD SIMULATIONS

A further evaluation of the intensity of contrasts of clear and cloudy areas on mesoscale circulations was performed by assuming a relatively short period of cloudy–clear area contrasts, beginning at various hours of the day. The study by Wetzel et al. (1984), relating to the impact of short period cloud shading on the surface temperature, implies that possible significant thermal circulations are also associated with short-term contrasts. Three cases indicated as C10, C12 and C14 were considered in which cloud contrasts similar to those in case CCC were imposed at 1000, 1200 and 1400 LST, respectively, and lasted for two hours. (The simulations commenced at 0800 LST.) Prior to the insertion of clouds, a clear-sky PBL developed throughout the entire simulated domain. In Table 3 several typical features of the induced circulations in these cases are listed. Since the incoming solar radiation at the surface in the three simulations are almost identical, the related values of w_{max}, and u_{smax} are similar (although in the initiation of the different cloud contrast situations, different PBL heights were involved with the three cases). The values of u_{smax} and w_{max} are generally in the range of 50% to 75% of the equivalent values obtained in case CCC following 6 hours. The intensity of the surface line circulation, C_m, however, in this case is around 25% of that simulated in CCC. Thus, even for a relatively short duration, a cloud contrast around noon is expected to have a significant effect on the development of horizontal and vertical velocities. In addition, the horizontal extent of the circulation was found (not shown) to be much smaller in these cases as compared to the case CCC. This difference in the horizontal extent of the circulations is implied by Eq. (7).

5) SURFACE LINE CIRCULATIONS

In this subsection the surface line circulation C_m ($= \int_A^B u_s dl$), based on the model simulated surface flow, and C_a, the surface line circulation based on the scaling procedures suggested in section 2, are compared. In addition to evaluations of the scaling accuracy as compared to detailed model results, further insight into the relation between the thermal forcing and the induced circulation in our study is provided.

In the derivation of C_a, a linear increase from the initiation of the thermal contrast to the hour of its computation has been assumed. The Rayleigh friction constant α is adopted to be 2×10^{-3} s^{-1} over the land domain and 0.5×10^{-3} s^{-1} over water surfaces which

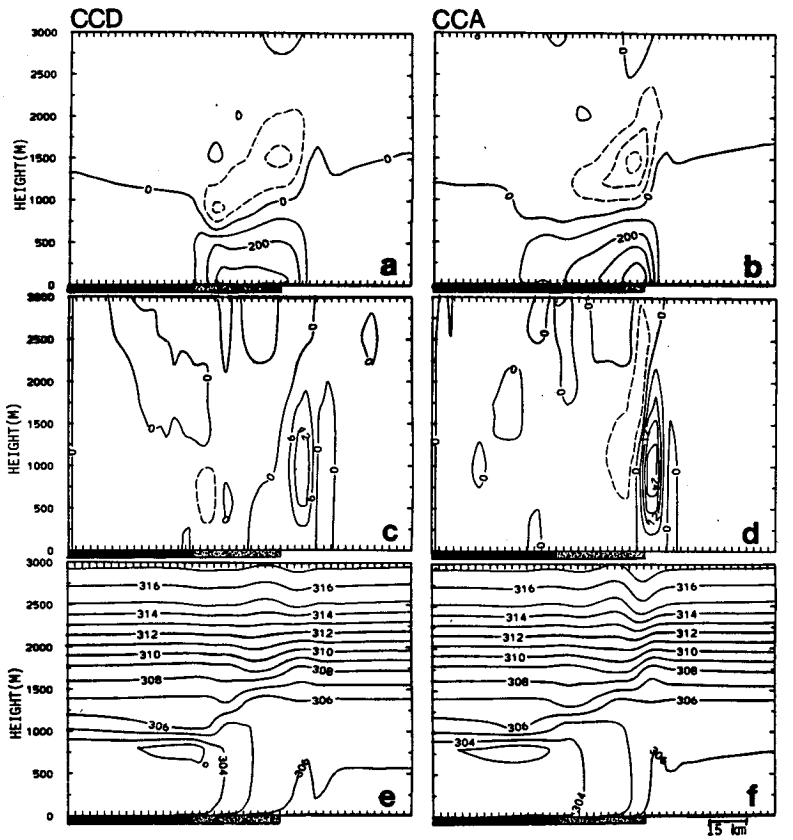

FIG. 7. As in Fig. 6 except for cases CCD (dotted segment indicates the region involved with cloud dissipation during the period 0800–1400 LST) and CCA (dotted segment indicates the region along which the cloud was advected during the period 0800–1400 LST).

is, on the average, slightly higher than that suggested in Martin and Pielke (1983). Since surface sensible heat fluxes over water sections are negligible as compared to the land sections, it was assumed that $\bar{R}_s = 0$ over the water. Using (7) and (8), we note that the evaluation of C_a becomes straightforward if the solar radiation distribution is known.

Computed C_m and C_a values following time t from the initiation of the circulations are given in Table 3, showing, in general, reasonable agreement. The most developed surface circulation is that induced in the case SBN, which is about double that obtained in the cases SBC and CCC (as evident also from the surface wind speed and the horizontal extent of circulations presented earlier for these cases). In the 2-h period simulations (cases C10, C12 and C14) the values for C_m and C_a are almost identical for the three cases, due to similar values for the incoming solar radiation at the surface throughout the two hours in which the contrast was introduced. In the slope simulations (case SN and SC), the surface line circulations are evaluated along the same slope extent, demonstrating that the ratio of the averaged surface upslope wind speed in both cases (as indicated by Table 3) is the same as the ratio involved with the computed surface line circulations [as implied by (8)].

4. Discussion

The present study evaluated the impact of cloud shading on sea breeze and daytime thermally induced slope flows, as well as thermally induced circulations between clear and cloudy areas. Scaling and numerical model evaluations of simplified cases were performed which indicated the major impacts that cloud shading has on either altering or inducing the abovementioned circulations. Most noticeable are the following:

- Sea-breeze and thermally induced upslope circulation intensities may be reduced by as much as a factor of 2 when the incoming solar radiation at the surface is 40% of its value for clear-sky conditions. (Such a modification in the solar radiation at the surface is typical during overcasts.)
- Mesoscale, thermally induced circulations generated by a stagnant cloudy area contrasted by a clear

area may approach in their intensity and characteristics that of an equivalent sea breeze. Advecting the contrast line into the clear area with a slow speed, i.e., less than about 6 km h^{-1}, (which results in an expansion of the cloudy area) causes only a slight modification in the features simulated for the stagnant case. On the other hand, moving the contrast line which results in an expansion of the clear area (as caused by cloud dissipation or advection) tends to reduce the peak values of the generated velocities.

- Even a short duration of cloudy–clear area contrast can lead to the generation of a circulation which may be of meteorological importance in terms of the low-level wind.

The following suggestions for further generalizations of the results are made:

- Conceptually, the PBL characteristics involved with medium and high-level clouds can be satisfactorily described in a simple relation by considering its impact on the surface heating. This is not always the case with low clouds which cap the PBL (e.g., stratus or fair weather cumulus); in this case net longwave radiative cooling in and above the cloud layer alters and reduces the development of the PBL. This reduction is expected to be less as the cloud deck thickness becomes less. On the average, with relatively thick clouds, the temperature of the PBL is expected to be lower than that associated with a cloud-capped PBL where the longwave radiative cooling is not considered. Therefore, in this case further intensification of the features obtained in the analysis and the simulations presented in this paper should be expected.
- Cloudy atmospheres may be associated with relatively strong synoptic flows. These flows are likely to distort, to some extent, the circulation patterns typical for a nearly calm atmosphere, as assumed for the calculations presented in this paper. Evaluation of the variety of situations involved with synoptic flows was not made here since the current study is oriented toward basic, idealized situations. However, using the knowledge obtained in many studies relating to synoptic flow interactions with the sea breeze or thermally induced upslope flows (examples of such studies are listed in Ookouchi et al., 1984), it is possible to project and evaluate such interactions from the cases simulated in the present study.

Finally, studies such as the ones presented here are of importance as we attempt to gain a better understanding of all types of thermally forced circulations which may have a significant impact on the mesoscale environment. With GOES data, routine 30-min interval observations exist every 1 km using the information in the visible data and every 8 km with infrared data. In mid-1986, the GOES satellite system will provide routine thermodynamic information at 14-km resolution (in clear areas) using its atmospheric sounding capability. Such data will most likely be available at an interval between one and three hours. Model studies such as the present one, including further refinements, may be adopted to test and devise methodologies for using such high resolution data sets. One may envision this study as an initial step toward inserting satellite cloud cover information (type, brightness, size, advection, etc.) into a mesoscale model for real-time nowcast applications.

Acknowledgments. The study was supported by the NSF under Grant ATM-8414181 and by NASA under Grant NAG 5-359. The computations were carried out by the NCAR CRAY computer. (NCAR is sponsored by the National Science Fondation.) We would like to thank Chaing Chen and Yasumasa Ookouchi for useful discussions, and Liz Lambert, Sandy Page, and Sara Rumley for editing and typing the manuscript.

REFERENCES

Abbs, D. J., 1984: Observations and numerical modelling of southern Australian sea breezes. Ph.D. dissertation, Dept. of Meteorology, University of Melbourne, Australia, 308 pp.

Anthes, R. A., 1978: The height of the planetary boundary layer and the production of circulation in a sea breeze model. *J. Atmos. Sci.*, **35**, 1231–1239.

Bailey, M. J., K. M. Carpenter, L. R. Lowther and C. W. Passant, 1981: A mesoscale forecast for 14 August 1975—the Hampstead storm. *Meteor. Mag.*, **110**, 147–161.

Banta, R. M., 1984: Daytime boundary-layer evolution over mountainous terrain. Part I: Observations of the dry circulations. *Mon. Wea. Rev.*, **112**, 340–356.

Carpenter, K. M., 1982: Model forecasts for locally forced mesoscale systems. *Nowcasting*, K. A. Browning (Ed.), Academic Press, 223–234.

Dirks, R. A., 1969: A climatology of central Great Plains mesoscale convective systems. Tech. Rept. E-10-686. Dept. of Atmospheric Sciences, Colorado State University, Fort Collins, 60 pp.

Gannon, P. T., 1978: Influence of earth surface and cloud properties on the South Florida sea breeze, NOAA Tech. Rep., ERL 402-NHEML-2, U.S. Dept. of Commerce, 91 pp.

Gurka, J. J., 1978: The role of inward mixing in the dissipation of fog and stratus. *Mon. Wea. Rev.*, **106**, 1633–1635.

Klitch, M. A., J. F. Weaver, F. P. Kelly and T. H. Vonder Haar, 1985: Convective cloud climatologies constructed from satellite imagery. *Mon. Wea. Rev.*, **113**, 326–337.

Liou, K-M., 1976: On the absorption, reflection, and transmission of solar radiation in cloudy atmosphere. *J. Atmos. Sci.*, **33**, 798–805.

McNider, R. T., and R. A. Pielke, 1981: Diurnal boundary-layer development over sloping terrain. *J. Atmos. Sci.*, **38**, 2198–2212.

——, G. J. Jedlover and G. S. Wilson, 1984: Data analysis and model simulation of the initiation of convection on April 24, 1982. Tenth Conf. on Weather Forecasting and Analysis, Tampa. Amer. Meteor. Soc., 543–549.

Mahrer, Y., and R. A. Pielke (1977): A numerical study of air flow over irregular terrain. *Contrib. Atmos. Phys.*, **50**, 98–113.

Martin, C. L., and R. A. Pielke, 1983: The adequacy of the hydrostatic assumption in sea breeze modeling over flat terrain. *J. Atmos. Sci.*, **40**, 1472–1481.

Neumann, J., and Y. Mahrer, 1974: A theoretical study of the sea and land breeze of circular islands. *J. Atmos. Sci.*, **31**, 2027–2039.

Nicholls, S., 1984: The dynamics of stratocumulus: Aircraft observations and comparisons with mixed-layer model. *Quart. J. Roy. Meteor. Soc.*, **110,** 783–820.

Oke, T. R., 1978: *Boundary Layer Climates,* Methuen, 372 pp.

Ookouchi, Y., M. Segal, R. C. Kessler and R. A. Pielke, 1984: Evaluation of soil moisture effects on the generation and modification of mesoscale circulations. *Mon. Wea. Rev.*, **112,** 2281–2292.

Pielke, R. A., 1974: A three-dimensional numerical model of the sea breezes over south Florida. *Mon. Wea. Rev.*, **102,** 115–139.

——, and Y. Mahrer, 1978: Verification analysis of the University of Virginia three-dimensional mesoscale model prediction over south Florida for July 1, 1973. *Mon. Wea. Rev.*, **106,** 1568–1589.

Purdom, J. F. W., 1982: Subjective interpretation of geostationary satellite data for Nowcasting. *Nowcasting,* K. A. Browning, Ed., Academic Press, 149–166.

——, and J. G. Gurka, 1974: The effect of early morning cloud cover on afternoon thunderstorm development. *Fifth Conference on Weather Forecasting and Analysis.* St. Louis, Amer. Meteor. Soc., 58–60.

Segal, M., and R. A. Pielke, 1981: Numerical model simulation of biometerological heat load condition-summer day case study for the Chesapeake Bay Area. *J. Appl. Meteor.*, **20,** 735–749.

——, Y. Mahrer and R. A. Pielke, 1982: Application of a numerical mesoscale model for the evaluation of seasonal persistent regional climatological patterns. *J. Appl. Meteor.*, **21,** 1754–1762.

——, ——, and ——, 1983: A numerical model study of the meteorological patterns induced by a lake confined by mountains-the Dead Sea case. *Quart. J. Roy. Meteor. Soc.*, **109,** 549–564.

Simpson, J. E., D. A. Mansfield and J. R. Milford, 1977: Inland penetration of sea breeze fronts. *J. Roy. Meteor. Soc.*, **103,** 47–76.

Stephens, G. L., 1984: The parameterization of radiation for numerical weather prediction and climate models. *Mon. Wea. Rev.*, **112,** 826–867.

Tennekes, H., 1973: A model for the dynamics of the inversion above a convective boundary layer. *J. Atmos. Sci.*, **30,** 558–567.

Wallace, J. M., 1975: Diurnal variations in precipitation and thunderstorm frequency over the conterminous United States. *Mon. Wea. Rev.*, **103,** 406–419.

Weiss, C. E., and J. F. W. Purdom, 1974: The effect of early morning cloud cover on squall line activity. *Mon. Wea. Rev.*, **102,** 400–401.

Wetzel, P. J., D. Atlas and R. H. Woodward, 1984: Determining soil moisture from geosynchronous satellite infrared data: A feasibility study. *J. Climate Appl. Meteor.*, **23,** 375–391.